Journal of Environmental Radioactivity 171 (2017) 21–33

Contents lists available at ScienceDirect

Journal of Environmental Radioactivity

journal homepage: www.elsevier.com/locate/jenvrad

Modeling watershed-scale ^{137}Cs transport in a forested catchment affected by the Fukushima Dai-ichi Nuclear Power Plant accident

Lezhang Wei [a, b, *], Tsuyoshi Kinouchi [a], Kazuya Yoshimura [c], Mark L. Velleux [d]

[a] Department of Environmental Science and Technology, Tokyo Institute of Technology, Japan
[b] Linköping University, Guangzhou University Research Center on Urban Sustainable Development, Guangzhou University, China
[c] Sector of Fukushima Research and Development, Japan Atomic Energy Agency, Japan
[d] HDR, USA

ARTICLE INFO

Article history:
Received 20 July 2016
Received in revised form
17 January 2017
Accepted 18 January 2017
Available online 3 February 2017

Keywords:
^{137}Cs transport
Fukushima nuclear accident
Forested catchment

ABSTRACT

The Fukushima nuclear accident in 2011 resulted in ^{137}Cs contamination of large areas in northeast Japan. A watershed-scale ^{137}Cs transport model was developed and applied to a forested catchment in Fukushima area. This model considers ^{137}Cs wash-off from vegetation, movement through soils, and transport of dissolved and particulate ^{137}Cs adsorbed to clay, silt and sand. Comparisons between measurements and simulations demonstrated that the model well reproduced ^{137}Cs concentrations in the stream fed from the catchment. Simulations estimated that 0.57 TBq of ^{137}Cs was exported from the catchment between June, 2011 and December, 2014. Transport largely occurred with eroded sediment particles at a ratio of 17:70:13 of clay, silt, and sand. The overall ^{137}Cs reduction ratio by rainfall-runoff wash-off was about 1.6%. Appreciable ^{137}Cs remained in the catchment at the end of 2014. The largest rate of ^{137}Cs reduction by wash-off was simulated to occur in subwatersheds of the upper catchment. However, despite relatively low initial deposition, middle portions of the watershed exported proportionately more ^{137}Cs by rainfall-runoff processes. Simulations indicated that much of the transported ^{137}Cs originates from erosion over hillsides and river banks. These results suggested that areas where ^{137}Cs accumulates with redeposited sediments can be targeted for decontamination and also provided insight into ^{137}Cs transport at the watershed scale to assess risk management and decontamination planning efforts.

1. Introduction

The Fukushima Dai-ichi Nuclear Power Plant (FDNPP) accident in 2011 released an estimated 1–2 × 10^4 TBq of ^{137}Cs to the atmosphere (IAEA, 2011). Cesium-137 persists in the environment because of its long half-life (30.2 years). Airborne surveys and other studies showed that fallout radionuclides were deposited throughout Japan and elsewhere across the world, in particular, areas northwest of the FDNPP were heavily contaminated (MEXT, 2013; Stohl et al., 2012; Masson et al., 2011). As a consequence of direct radiation exposure risks and potential transfer to plants and animals through food chains (Taira et al., 2012; Kanasashi et al., 2015; Ayabe et al., 2014; Sato et al., 2014; Harada et al., 2013), the transport and fate of ^{137}Cs is a public health and environmental management concern.

Monitoring and soil sampling efforts conducted after the accident (MEXT, 2013; Kobayashi et al., 2015; Saito et al., 2015; Sanada and Torii, 2015) have provided information regarding patterns of ^{137}Cs occurrence at discrete points in time. In combination with these data, physically-based watershed models are useful to examine ^{137}Cs transport dynamics, identify sources and sinks, estimate future conditions, and evaluate decontamination alternatives. Although various models were developed to investigate the transport and fate of radioactive substances from nuclear accidents in Chernobyl (Monte, 2001; van der Perk and Slávik, 2003) and Fukushima (Yamaguchi et al., 2013; Yamaguchi et al., 2014; Kitamura et al., 2014; Kinouchi et al., 2015; Tanaka et al., 2013), those prior models either did not account for ^{137}Cs interaction with vegetation layers, or neglected ^{137}Cs sorption to the range of particle sizes in soils, transport of the dissolved phase, and the short-term and event-driven nature of episodic erosion and transport.

* Corresponding author.Department of Environmental Science and Technology, Tokyo Institute of Technology, Japan.
E-mail address: bjyq_2006@126.com (L. Wei).

http://dx.doi.org/10.1016/j.jenvrad.2017.01.017
0265-931X/

The radionuclide transport through a catchment is governed by two main classes of processes (Kivva and Zheleznyak, 2000): hydrological processes and physical-chemical processes. The former one, which involves water flow and sediment erosion, transport and deposition, controls ^{137}Cs transport at the watershed scale. In addition to dry deposition, radiocesium is scavenged from the atmosphere with precipitation (Stohl et al., 2012). A large portion of ^{137}Cs fallout was intercepted by vegetation (canopy and litter layers) and slowly washed out over time (Shaw, 2007; Kato et al., 2012; FAJ, 2012), particularly in forested areas. At the ground surface, ^{137}Cs can move downward through soils with infiltrating water or move across the landscape as particulate or dissolved phase, and subsequently move through river systems (Takahashi et al., 2015; Yamashiki et al., 2014). Soil and sediment composition is an important factor because radionuclide sorption to particles is size-dependent, with preferential sorption to finer particles because of their higher specific surface areas (He and Walling, 1996; Tanaka et al., 2014; Yamashiki et al., 2014). Moreover, models must be able to simulate transport dynamics with fine time steps because extreme events periodically mobilize large quantities of solids and associated radionuclides in very short timeframes. Studies show that more than 60% of radiocesium exported from the Abukuma River watershed over a 9-month period occurred in just 2 d during Typhoon Roke (September 21–22, 2011) (Yamashiki et al., 2014), and radiocesium flux during that typhoon event accounted for 30%–50% of the annual flux from the Natsui and Same Rivers (Nagao et al., 2013). The physical-chemical processes of radioactive substances mean the interaction processes between radionuclides in dissolved form with the rocks in catchments, and in particular, with soil particles (Kivva and Zheleznyak, 2000). Although particulate transport is predominant (Ueda et al., 2013), dissolved transport cannot be entirely neglected because dissolved ^{137}Cs should be of critical importance regarding its uptake by aquatic organisms (Sakaguchi et al., 2014; Sasaki et al., 2016).

Given these considerations, the objectives of the present study are: (1) to develop a watershed-scale transport model that considers ^{137}Cs interaction with vegetation, partitioning from dissolved form to particles with multiple sizes, and transport at time scales commensurate with episodic transport during large events; and (2) apply the model to the Kuchibuto River catchment as a case study to assess hydrological processes that control transport of radiocesium resulting from the FDNPP accident.

2. Model description

Our ^{137}Cs transport model is based on the TREX framework (Velleux et al., 2008). TREX is a physically-based, spatially distributed, watershed-scale, rainfall–runoff, sediment transport, and chemical transport model that features two-dimensional flow routing overland, flow through a nest network of channels, and the capability to simulate sediment erosion and transport with multiple size classes. This type of model has been used in flood forecasting (England et al., 2007), soil erosion research (Rojas et al., 2008; Ji et al., 2014), and analysis of contaminant transport and fate (Velleux et al., 2006, 2008, 2012).

2.1. Hydrological and soil erosion and transport model

The hydrological module of TREX was derived from the work of Julien and Saghafian (1991), Julien et al. (1995) and Julien and Rojas (2002). The major components of the model include: rainfall, interception and evapotranspiration, surface storage, infiltration, subsurface and groundwater flow, and overland and channel runoff routing (Velleux et al., 2008; Wei and Kinouchi, 2014). The Green and Ampt equation is used to represent infiltration. Lateral and vertical subsurface flows are calculated by a kinematic storage model and a storage routing method, respectively. A linear reservoir method is used to calculate groundwater flow. Overland flow is simulated in two dimensions using the diffusive wave approximation. In floodplain areas, water and transported constituents (e.g. sediment, chemical substances) are transferred between the overland plane and channel network based on the difference in water surface elevations. Channel flow is simulated in one dimension using the diffusive wave approximation. Manning formulation is used to solve the overland and channel flow equations.

The soil erosion and sediment transport module is driven by overland and channel flows and includes processes for erosion and deposition. Soil erosion on the upland includes rainfall splash erosion and water flow erosion (Woolhiser et al., 1990). Splash erosion of soils is approximated as a function of the square of rainfall rate. Water flow erosion is a function of transport capacity. Multiple particle size classes such as clay, silt, and sand can be simulated (Velleux et al., 2008; Ji et al., 2014; Wei et al., submitted). Sediment deposition is determined by the settling velocity of each particle type (solid particles with different diameters) and its probability of deposition.

2.2. Cesium-137 transport model

Fig. 1 shows a schematic of computations that occur in each model cell. Initial conditions are established by dividing the ^{137}Cs inventory for each cell into portions that are deposited onto vegetation (k_v) or bare soil (1-k_v). During precipitation, ^{137}Cs trapped by vegetation is washed off gradually (J_v) and accumulates at the soil surface, infiltrate, or be transported with overland flow depending on its phase and runoff conditions in the cell. Cesium-137 in overland water can be advected along with surface runoff. In the

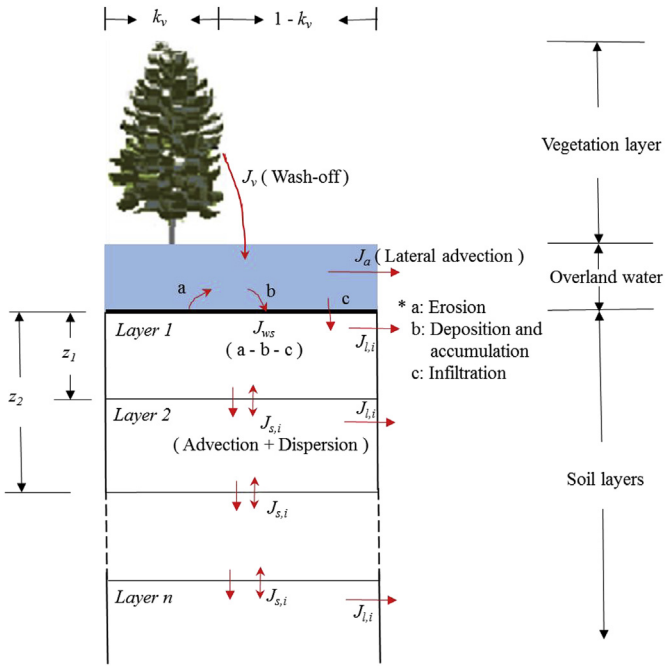

Fig. 1. Schematic diagram of ^{137}Cs migration in each computational cell. (k_v, fraction of vegetation; z_i, z_{i+1}, upper and lower boundary depth of layer i, respectively; J_v, ^{137}Cs loss in vegetation layer; J_{ws}, ^{137}Cs transport flux associated with (a) soil erosion and (b) deposition including ^{137}Cs accumulation to the top soil layer when no runoff is generated in addition to (c) dissolved ^{137}Cs to soil along with water infiltration; J_a, lateral ^{137}Cs advection with surface runoff; $J_{l,i}$, dissolved ^{137}Cs transport along with subsurface flow, $J_{s,i}$, ^{137}Cs advection and dispersion in soil layers.).

surface soil layers, the ^{137}Cs transport flux (J_{ws}) involves several processes: erosion (a), deposition (b) and dissolved phase infiltration (c). The model considers ^{137}Cs vertical transport between soil layers due to precipitation, soil animal activities and other factors.

2.2.1. Initial ^{137}Cs distribution

In each computational cell, ^{137}Cs was assumed to be distributed in two components, i.e. vegetation layer and soil layers. The portion of the initial ^{137}Cs inventory intercepted by the vegetation layer is:

$$I_{0_c} = k_v f_c I_0 \tag{1}$$

The remaining portion of the initial inventory reaching the soil matrix is:

$$I_{0_s} = I_0 - I_{0_c} = (1 - k_v f_c) I_0 \tag{2}$$

where I_{0c} is the initial ^{137}Cs trapped by vegetation (Bq/m^2); I_{0s} is the initial ^{137}Cs inventory in soil layers (Bq/m^2); I_0 is the total ^{137}Cs inventory at the start of the simulation as measured by airborne survey (Bq/m^2); k_v is the fraction of vegetative cover in each cell (dimensionless); and f_c is the initial fraction of ^{137}Cs fallout trapped in vegetation (dimensionless). Parameters in this study were summarized in the supplementary material S.1.

The initial distribution of ^{137}Cs concentrations in soils is given by an exponential function of soil depth z and the initial inventory (Takahashi et al., 2015), and can be estimated by (Kinouchi et al., 2015):

$$C_{cb}(0) = \frac{k I_{0_s}}{\rho_s \left[1 - e^{-k z_0}\right]} \tag{3}$$

$$C_{cb}(z) = C_{cb}(0) e^{-kz} \tag{4}$$

where $C_{cb}(0)$ is the ^{137}Cs concentration at the soil surface (z = 0) (Bq/g); C_{cb}(z) is the ^{137}Cs concentration at depth z (Bq/g); k is an attenuation coefficient (1/m); ρ_s is soil dry bulk density (kg/m^3); and z_0 is the depth interval of measurements used to determine ^{137}Cs concentrations in the soil (= 0.05 m).

Thus, the average concentration in each soil layer of the model is:

$$C_{cb,i} = \rho_s \frac{1}{z_{i+1} - z_i} \int_{z_i}^{z_{i+1}} C_{cb}(z) dz \tag{5}$$

where $C_{cb,i}$ is the ^{137}Cs concentration in the soil layer i (Bq/m^3); and z_i, z_{i+1} are the upper and lower boundary depths of layer i, respectively.

2.2.2. Cesium-137 loss from the vegetation layer

Radiocesium retained in the vegetation layer is lost by radioactive decay and processes such as weathering by rainfall, wind, dew, translocation, and other factors. This decrease after decay correction is known as field loss and is time-dependent reduction described by a rapid initial loss followed by a slower loss (Milbourn and Taylor, 1965; Chadwick and Chamberlain, 1970; Madoz-Escande et al., 2005; Fraley et al., 1993). Loffredo et al. (2014) reported that field loss of ^{137}Cs in Fukushima was strongly influenced by rainfall. In the present study, we assumed that ^{137}Cs loss from vegetation has fast and slow components and can be modeled by a double exponential model (Ertel et al., 1989; Loffredo et al., 2014). Field loss of ^{137}Cs from the vegetation layer was estimated as:

$$J_v = k_v A_s i_n C_p \tag{6}$$

where J_v is ^{137}Cs loss from the vegetation layer (Bq/s); A_s is surface area of a computational cell (m^2); i_n is net rainfall intensity (mm/s); and C_p is the ^{137}Cs inventory loss per net rainfall (Bq/m^2/mm), which is calculated as:

$$C_p = C_v \frac{I_{oc}}{1 + \frac{1}{r_{12}}} \left(\frac{1}{r_{12}} \lambda_f e^{-\lambda_f t} + \lambda_s e^{-\lambda_s t} \right) \tag{7}$$

where C_v is a coefficient (1/mm); r_{12} is the ratio between ^{137}Cs inventory for slow and fast loss (= 0.22) (Loffredo et al., 2015); λ_f and λ_s are constants for fast and slow loss, respectively (1/s); t is the elapsed time from the initial condition. Cesium-137 storage in the vegetation layer is updated over time as:

$$I_{c,t_2} = I_{c,t_1} - \frac{J_v}{A_s} \Delta t \tag{8}$$

where I_c is ^{137}Cs storage in the vegetation layer (Bq/m^2); subscripts t_1 and t_2 refer to the beginning and end of the time periods for numerical integration, respectively, and $\triangle t$ is the numerical integration time step (s).

2.2.3. Cesium-137 phases in water

Cesium-137 transport and interactions depend on chemical phase. Radionuclide partitioning between water and suspended matter is generally described in terms of a distribution coefficient that is expressed as the ratio of concentrations in the particulate and dissolved phase (Sheppard et al., 2009; Ueda et al., 2013). The distribution coefficient of ^{137}Cs is defined as:

$$f_d = \frac{1}{1 + \sum_{n=1}^{N} m_n K_{d,n}} \tag{9}$$

$$f_{p,n} = \frac{m_n K_{d,n}}{1 + \sum_{n=1}^{N} m_n K_{d,n}} \tag{10}$$

where f_d is the fraction of ^{137}Cs in the dissolved phase (dimensionless); $f_{p,n}$ is the fraction of ^{137}Cs in the particulate phase associated with solid particle n (dimensionless); $K_{d,n}$ is the distribution coefficient of chemical to solid particle n (m^3/kg); m_n is the concentration of solid particle n (kg/m^3); and n is the index for each solid particle type simulated. Three types of solid (i.e. clay, silt and sand), to which ^{137}Cs adsorbed, are considered in this study.

2.2.4. Cesium-137 transport in overland flow

Cesium-137 in overland flow in each cell is supplied from field loss of the vegetation layer and eroded sediments from the underlying soil matrix. Depositing solids carry particulate ^{137}Cs to the soil matrix. Dissolved ^{137}Cs infiltrates into the soil matrix. For periods when no overland flow is generated, ^{137}Cs washed from vegetation accumulates in the top soil. Overland flow transports ^{137}Cs from cell to cell in the lateral direction. The mass balance of ^{137}Cs in the water column of the overland plane is calculated by:

$$\frac{\partial C_{c,ov}}{\partial t} = \frac{J_v + J_{ws} - \Delta J_a}{V_w} \tag{11}$$

$$J_{ws} = A_s \left(\sum_{n=1}^{N} v_r C_{cb,1} f_{pb,n} - \sum_{n=1}^{N} v_{se} C_{c,ov} f_{p,n} - v_i C_{c,ov} f_d \right) \tag{12}$$

$$J_a = \left(A_c v_x + A_c v_y + A_c v_f \right) C_{c,ov} \tag{13}$$

where $C_{c,ov}$ is the total ^{137}Cs concentration in the water column (Bq/m^3); J_{ws} is the ^{137}Cs transport flux associated with erosion, deposition, and dissolved ^{137}Cs infiltration to the top soil layer, which also includes ^{137}Cs accumulation by washing-off from vegetation when no overland flow is generated (Bq/s); $\triangle J_a$ is the net flux, which is the difference of ^{137}Cs lateral flowing out (J_a) and flowing in the computation cell; $C_{cb,1}$ is the total ^{137}Cs concentration in the first soil layer (Bq/m^3); A_c and A_s are the cross-sectional area in the flow direction and surface area, respectively (m^2); $f_{p,n}$ is the particulate ^{137}Cs fraction in the water column associated with particle type "n" (dimensionless); $f_{pb,n}$ is the particulate ^{137}Cs fraction in the first soil layer associated with particle type "n" (dimensionless), which is also calculated by Eq. (10); v_r, v_{se}, and v_i are soil erosion, deposition, and water infiltration velocities, respectively (m/s); v_x, v_y, and v_f are flow velocity in the x- or y-direction and between the overland plane and channel (floodplain), respectively (m/s); and V_w is the volume of water (m^3).

2.2.5. Cesium-137 transport in river channels

Cesium-137 can be transported from the overland plane to the channel network (or vice versa) with water flow in the floodplain. The ^{137}Cs transport processes in the river channel are analogous to those in overland areas:

$$\frac{\partial C_{c,ch}}{\partial t} = \left[\sum_{n=1}^{N} v_r C_{cb,ch} f_{pb,n} - \sum_{n=1}^{N} v_{se} C_{c,ch} f_{p,n}\right]\frac{A_s}{V_w} + v_f C_{c,ov}\frac{A_c}{V_w} - v_x C_{c,ch}\frac{A_c}{V_w} \quad (14)$$

$$\frac{\partial C_{cb,ch}}{\partial t} = \left[\sum_{n=1}^{N} v_{se} C_{c,ch} f_{p,n} - \sum_{n=1}^{N} v_r C_{cb,ch} f_{pb,n}\right]\frac{A_s}{V_s} \quad (15)$$

where $C_{c,ch}$ is the total ^{137}Cs concentration in the water column of the river channel (Bq/m^3); $C_{cb,ch}$ is the total ^{137}Cs concentration in the underlying sediment (Bq/m^3); v_x is flow velocity in the x-direction in the river channel (m/s), and v_f is the flow velocity between the overland plane and channel (floodplain) (m/s).

2.2.6. Cesium-137 in soils and sediments

Particulate ^{137}Cs in the topmost soil or sediment layer can be transported with particles as erosion and deposition occurs. Dissolved ^{137}Cs will be transported into the surface soil layer with infiltrating water and move through deeper soils layers with subsurface flow. The mass balance for soil and sediment layers is calculated by

$$\frac{\partial C_{cb,i}}{\partial t} = \frac{-J_{ws} + \Delta J_{s,i} - \Delta J_{l,i}}{V_s} \quad (16)$$

where i is the layer index of the soil/sediment bed; V_s is the volume of the soil/sediment layer (m^3); $\triangle J_{s,i}$ is the net ^{137}Cs vertical advection and dispersion flux in soil layer i (Bq/s). The vertical advection and dispersion flux ($J_{s,i}$) from soil layer is calculated by:

$$J_{s,i} = A_s\left(v_{adv} C_{cb,i} - \frac{E}{\Delta z}\left(C_{cb,i} - C_{cb,i+1}\right)\right) \quad (17)$$

where v_{adv} is ^{137}Cs vertical advection velocity (m/s); E is ^{137}Cs dispersion coefficient (m^2/s); $C_{cb,i}$, $C_{cb,i+1}$ are the ^{137}Cs concentration in the soil layers i *and* i+1, respectively; and $\triangle z$ is thickness of the soil layer i. Similarly, $\triangle J_{l,i}$ is the net dissolved ^{137}Cs lateral transport along with subsurface flow in soil layers (Bq/s):

$$J_{l,i} = A_c v_l C_{cb,i} f_{db} \quad (18)$$

where v_l is the lateral flow velocity from soil (m/s), and f_{db} is the dissolved ^{137}Cs fraction in the soil or sediment layer (dimensionless), which is calculated by Eq. (10).

The only transformation process in the model is radioactive decay, which was simulated as exponential decay over time according to the half-life (i.e. 30.2 y).

In this study three scenarios were simulated to clarify effects of different factors on radioactive substances transport in a forested watershed: scenario 1 considered the effect of vegetation and ^{137}Cs downward movement; scenario 2 and scenario 3 only considered one of them respectively.

3. Study area and data

The study area is the Kuchibuto River catchment, a forested catchment with an area of 137 km^2 in headwaters of the Abukuma River watershed that is located about 33–49 km northwest of the FDNPP (Fig. 2). Upstream areas of the catchment are within the exclusion zone established near the FDNPP.

A SRTM-based 90-m Digital Elevation Model (DEM) was downloaded (http://glcf.umd.edu/data/srtm/) and used to generate slope, flow direction, flow accumulation, river links and sub catchments (Fig. 3). River channel geometry (width, bank height, etc.) was defined as measured by a field survey. Elevations range from 200 m to 1000 m and the average slope is about 9.19°.

Land use and soil data were obtained from the Japan Ministry of Land, Infrastructure, Transport, and Tourism (MLIT) (http://nlftp.mlit.go.jp/ksj/). There are three predominant land use classes in the catchment: forest, cropland, and paddy field (Fig. 4). Four predominant soil types derived from granitic parent materials cover the catchment: Andosol soil (Kuroboku soil), granitic forest soil, lowland soil, and gley soil. Land use and soil properties have been estimated as part of a previous study (Kinouchi and Musiake, 2008). The native resolution of land use and soil type data are about 100-m and 1000-m, respectively. Land use and soil type data were downscaled to 90-m resolution using the majority resampling method within ArcGIS software. Use of a 90-m grid resolution was the result of a balance between the native resolution of data describing site topography, soils, and land use, computational burden, and the potential for introducing bias during model parameterization. Although categorical data for soil type and land use can be upscaled or downscaled without significant bias, topographic and soil erosion parameters may become less reliable at substantially coarser grid resolutions (Rojas et al., 2008).

Radar precipitation data from the Japan Meteorological Agency (JMA) was used to specify rainfall inputs. During simulations, rainfall was read every 30 min on a 1 km × 1 km grid, which is the native resolution of radar data. Flow and suspended sediment (SS) concentration have been measured at the downstream site and at the middle stream site (Fig. 2) since June 21, 2011 (Kinouchi et al., 2015; Yamashiki et al., 2014). Water samples from river sites and sediments trapped by time-integrated samplers (Phillips et al., 2000) were collected at the downstream site during a certain period (one to several weeks), and measurement results of part of samples has been published by Kinouchi et al. (2015). In this study, ^{137}Cs concentrations of the remaining samples were measured in a lab with a high-purity germanium gamma-ray well detector (GCW2022S, Canberra–Eurisys, Meriden, USA.) equipped with an amplifier (PSC822, Canberra, Meriden, USA.), and a multichannel analyzer (DSA1000, Canberra, Meriden, USA). The counting efficiency was calibrated using standard gamma sources: ^{210}Pb and ^{137}Cs (EG-CUSTOM, Isotope Products Laboratories, USA), ^{241}Am, ^{109}Cd, and ^{152}Eu (EG-CUSTOM, Eckert and Ziegler Isotope Products, USA) with different sample heights, and the analytical accuracy was certified via a World-Wide Proficiency Test by IAEA (IAEA, 2007). A

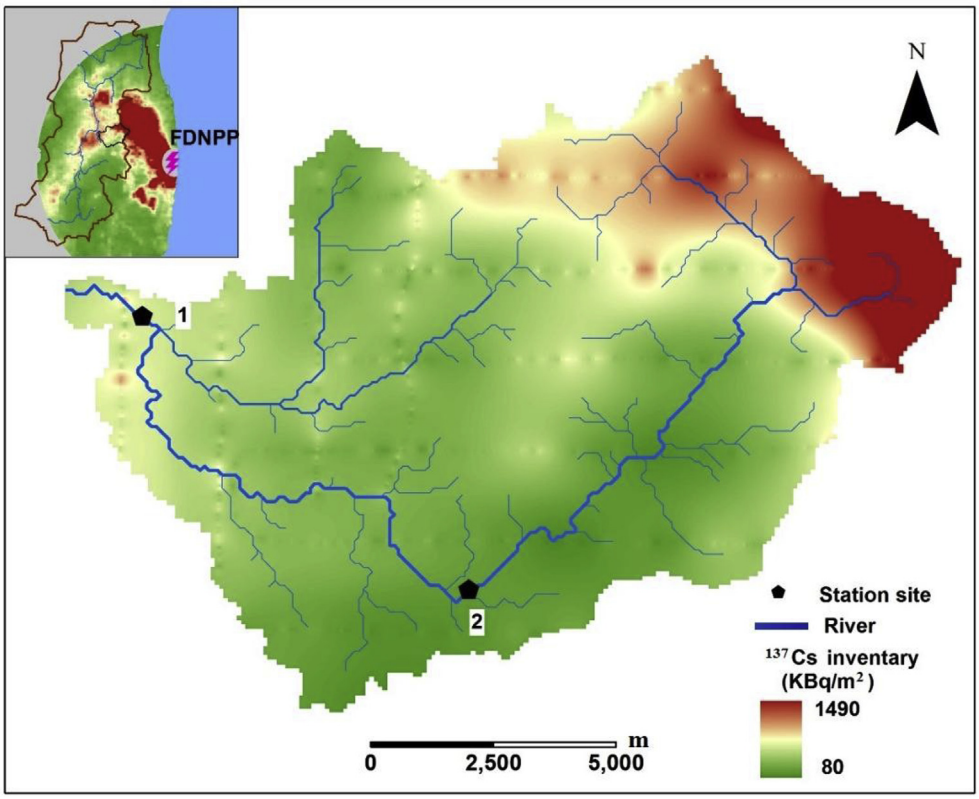

Fig. 2. ^{137}Cs distribution in the Kuchibuto River catchment. (1 and 2 indicate downstream and mid-stream sites, respectively. DEM: http://glcf.umd.edu/data/srtm/; ^{137}Cs distribution: MEXT, 2013).

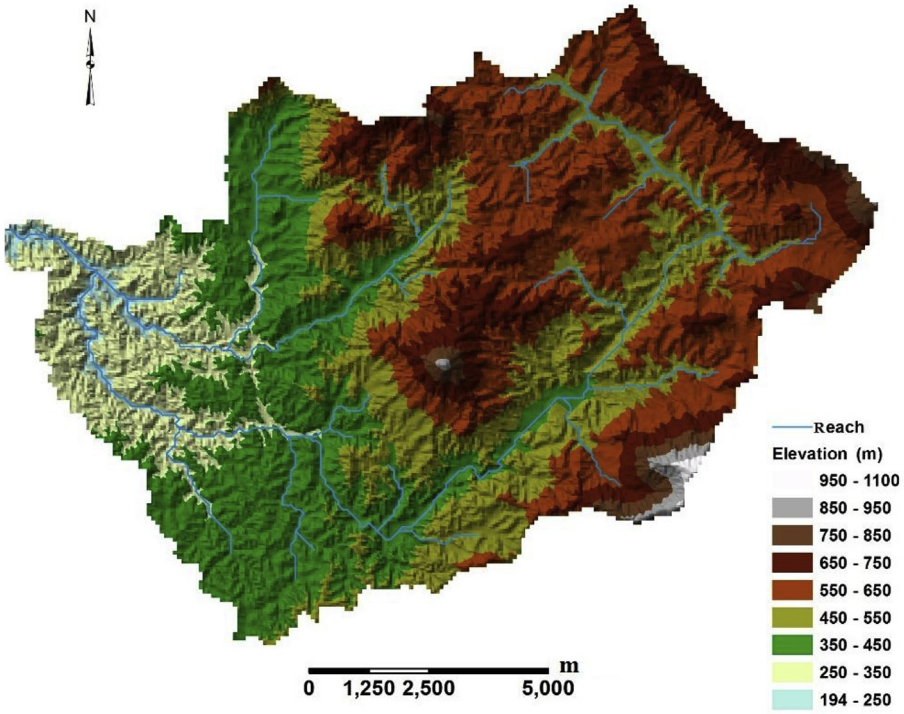

Fig. 3. Topographic characteristics of the Kuchibuto River catchment.

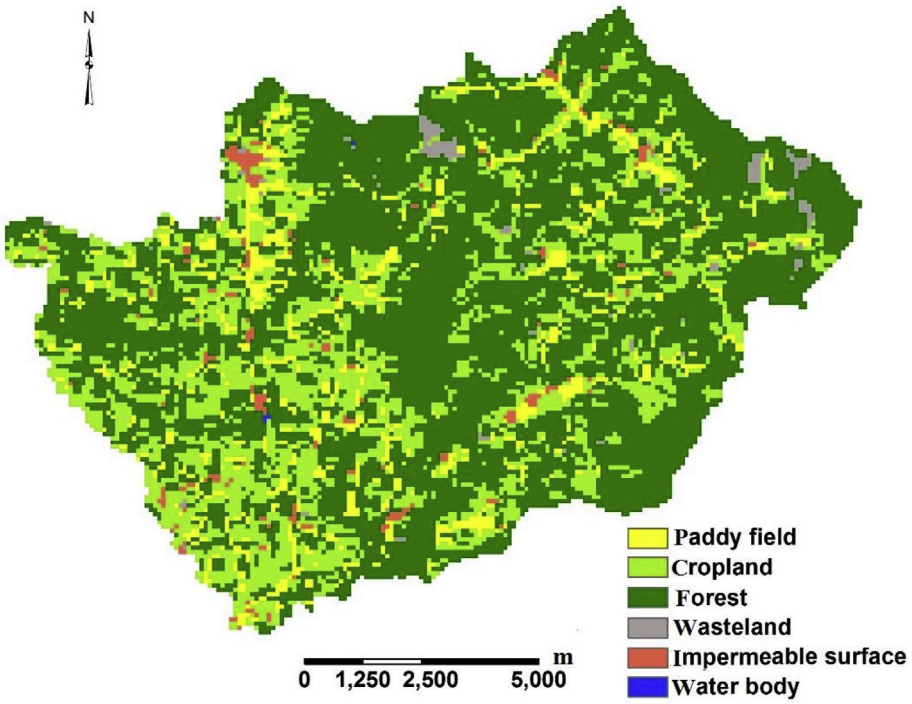

Fig. 4. Land use in the Kuchibuto River catchment (Land use: http://nlftp.mlit.go.jp/ksj/).

July 2, 2011 airborne survey (MEXT, 2013) (Fig. 2) was used to define the initial ^{137}Cs distribution for simulations.

Parameters related to hydrological and soil erosion and transport processes were measured or calibrated in previous studies (Kinouchi and Musiake, 2008; Wei and Kinouchi, 2014; Wei et al., submitted).

Several parameters in the model were determined based on prior field studies in this catchment. Distribution coefficients of ^{137}Cs ($K_{d,n}$) were set in Table 1 based on measurements in the Kuchibuto River (Fan et al., 2014). Ten layers, each with a thickness of 5 mm, were used to characterize ^{137}Cs distributions in the soil profile. The attenuation coefficient (k) and vertical advection velocities and dispersion coefficients (v_{adv}, E) varied according to land use type (Table 2) (Takahashi et al., 2015; JAEA, 2014). The area of the other land use types such as built-up land and water body are very small; thus, the ^{137}Cs in those areas assumed to be zero. A survey conducted by Forestry and Forest Products Research Institute (FFPRI) and Forestry Agency of Japan (FAJ) reported that about 20% of radiocesium was already in the soil matrix in the vegetation area by early August and September 2011 (FAJ, 2012). Thus, the fraction of ^{137}Cs trapped by vegetation in vegetation-covered areas (f_c) was set as 0.8 in our study. The parameters C_v and λ_f were calibrated to match measurements during June to September 2011, when rainfall is frequent and ^{137}Cs loss from vegetation is expected to be most prevalent (Table 3).

Table 1
K_d value for different solids (ml/g).

Clay (≤3 μm)	Silt (3–63 μm)	Sand (>63 μm)
$10^{6.2}$	$10^{6.0}$	$10^{5.8}$

Table 2
Parameters related to land use type.

Land use	k (1/cm)	v_{adv} (cm/year)	E (cm^2/year)
Paddy field	0.7	0.04	0.006
Cropland	1.2	0.04	0.006
Forest	0.6	0.09	0.016

k, v_{adv} and E were determined by referring prior field measurements (Takahashi et al., 2015; JAEA, 2014).

4. Results and discussion

The simulation period was June 21, 2011 to December 31, 2014. Three metrics were used to evaluate simulated flow rates and SS fluxes (Moriasi et al., 2007): Nash-Sutcliffe Efficiency (*NSE*), Root Mean Square Error standard deviation ratio (*RSR*), and Percent bias (*PBIAS*). The *NSE, RSR and PBIAS* for flow rate at the downstream sites were 0.88, 0.34 and −6%, respectively and for SS flux were 0.81, 0.44 and 4%, respectively (Fig. 5). Simulated water volume and total SS load (Fig. 6) were also in close agreement with measurements at the downstream sites for the simulation period.

4.1. Cesium-137 concentration at monitoring sites

Measured and simulated time-integrated particulate ^{137}Cs concentrations are presented in Fig. 7. Model results (shown as scenario 1) and measurements are in reasonable agreement except during November 2011 to March 2012, when particulate ^{137}Cs concentrations were underestimated. One possible cause is Aeolian transport and dry ^{137}Cs deposition. That period coincided with

Table 3
Parameters related to field loss.

C_v	λ_f	λ_s
0.05	3.5×10^{-2}	0.5×10^{-3}

λ_s was cited from Loffredo et al. (2015).

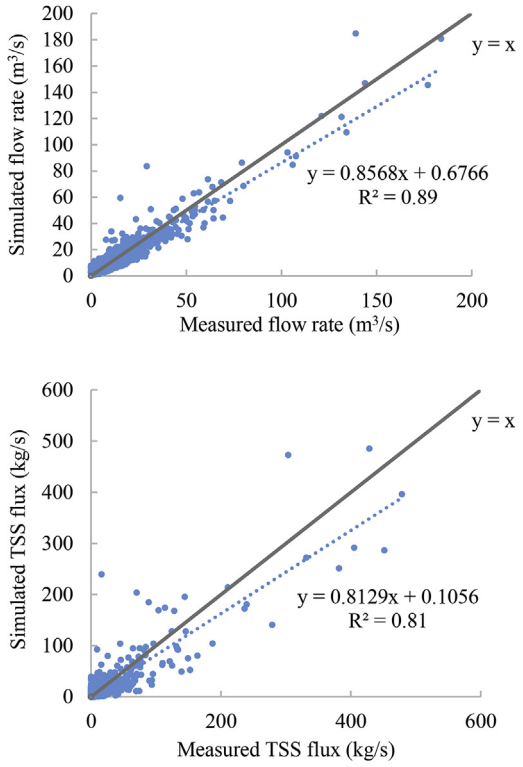

Fig. 5. Flow rates and total suspended sediment flux (TSS) at the downstream site (the regression lines were closed to the line y = x, representing good agreements of simulated and measured data).

winter and early spring, when winds are stronger than in other seasons. Strong winds could have transported ^{137}Cs from elsewhere in the watershed or from more heavily contaminated areas closer to Fukushima, and increased ^{137}Cs levels in the river. In addition to wind speed, transport with winds and dry deposition is influenced by factors such as wind direction, surface wetness. Concentrations of SS were also relatively small during this period and particulate ^{137}Cs concentrations would be sensitive to this dry ^{137}Cs deposition during that period. However, this underestimation bias in the model is negligible in terms of the annual ^{137}Cs load estimate because less than about 3% of annual ^{137}Cs load was transported from the catchment during November 2011 to April 2012 (Fig. 8). Over the period June 2011 to November 2013, the simulated total ^{137}Cs load of 0.45 TBq was quite close to the measured load of 0.44 TBq.

Instantaneous water samples from the river stations were collected during a storm on October 16, 2013, from which SS concentrations and particulate ^{137}Cs concentrations were measured. Measured and simulated particulate ^{137}Cs concentrations associated with different grain size fractions were plotted and compared with simulated data in Fig. 9. During the simulation period, the ratio of particulate ^{137}Cs flowing from the catchment carried by clay, silt, and sand was 17:70:13, respectively, whereas the ratio of flux for clay, silt, and sand was 7:65:28, respectively. Although some modeling studies were conducted in the Kuchibuto River catchment and other watersheds (Yamaguchi et al., 2014; Kitamura et al., 2014; Kinouchi et al., 2015; Tanaka et al., 2013), they did not provide such information, which possibly is useful for contamination control and understanding effects of radioactive substances on aquatic ecosystem.

Particulate ^{137}Cs concentrations in the Kuchibuto River decreased rapidly from June to September 2011 and then became relatively stable (Fig. 7). The fluctuation of the ^{137}Cs concentration in Fig. 7 reflects the common processes of watershed wash-off of atmospherically deposited radionuclides. At short time scales, watershed ^{137}Cs losses increase after heavy rainfalls, floods, and snowmelts. However, at long time scales (e.g. year), watershed wash-off losses generally decrease with time (Garcia-Sanchez, 2008). The concentration of ^{137}Cs at the downstream of the Kuchibuto River was about 1–10 Bq/g at the end of 2014 (Fig. 7). In contrast, pre-accident ^{137}Cs levels in soils at two sites in Fukushima were 0.558×10^{-3} to 48.4×10^{-3} Bq/g (Matsunaka et al., 2016). Therefore, it implies that, more than 3 y later, ^{137}Cs concentration in the Kuchibuto River was still 100 times higher than before the accident.

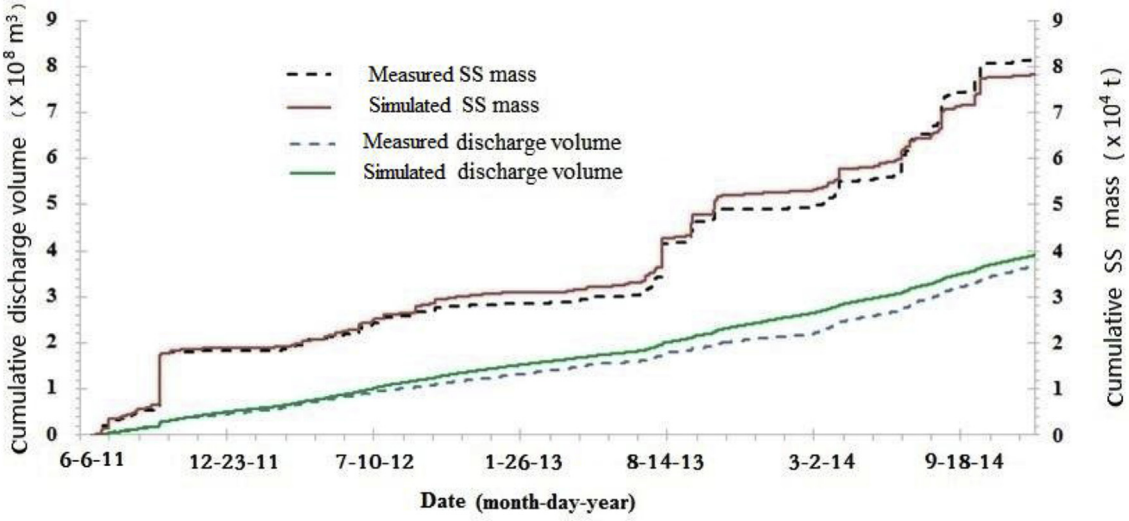

Fig. 6. Cumulative discharge volume and suspended sediment (SS) mass during the simulation period at the downstream site.
Scenario 1: includes ^{137}Cs wash-off from vegetation and downward movement through soils.
Scenario 2: includes ^{137}Cs downward movement through soil but excludes ^{137}Cs wash-off from vegetation with all ^{137}Cs adsorbed by surface soil particles.
Scenario 3: includes ^{137}Cs wash-off from vegetation but excludes ^{137}Cs downward movement through soil layers.

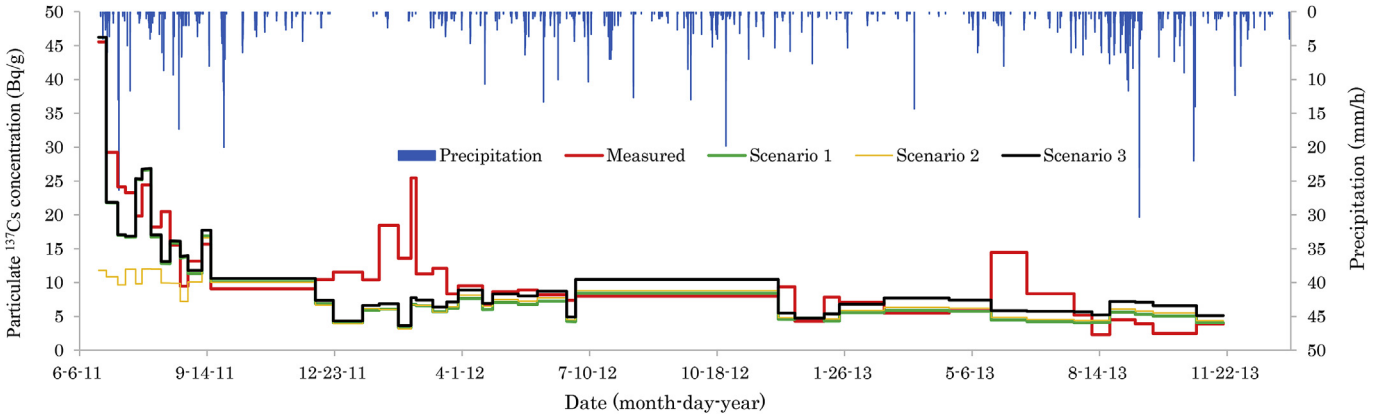

Fig. 7. Comparison of simulated and measured particulate ^{137}Cs concentration for three scenarios: downstream site (Data in this figure was listed in supplementary table S2.1).

4.2. Effects of vegetation and downward movement in soils

Differences between scenarios 1–3 in Fig. 7 illustrate the relative importance of these processes. When wash-off from vegetation is not included in the model, simulated particulate ^{137}Cs concentrations in the river are substantially lower than measured, during early stages of the simulation (scenario 2). This result confirms the speculation that leaching of radiocesium from the forest canopy probably played a significant role in transport of this radionuclide to the stream from the catchment during the initial period (Kinouchi et al., 2015).

Due to excluding the effect of downward migration, scenario 3 showed higher values than scenarios 1 and 2, and the differences increased over time. The trend of the differences implies that the necessity of inclusion of ^{137}Cs downward movement through soil in models depends on time scale of simulation. If a very short period is studied, ^{137}Cs downward movement through soil can be ignored. On the contrary, if the ^{137}Cs downward movement is not included for a long-term simulation (e.g. 30 y), ^{137}Cs transport from the catchment probably is overestimated.

4.3. Assessment of ^{137}Cs transport pathways

Fig. 10 shows ^{137}Cs transport in the vegetation–soil–river components for scenario 1. During the simulation period, ^{137}Cs field loss from the vegetation layer was about 2.36 TBq (2), and 4.85 TBq of ^{137}Cs remained in the layer at the end of the simulation. In our simulation, the retention ratio of the vegetation layer was 59% in mid-August, 2011, which was similar to the results of field study during the same period by Kato et al. (2012). They reported that in a coniferous forest in Tochigi Prefecture, Japan, an estimated 60% of the total deposited ^{137}Cs remained in the forest canopy 5 months after the accident. A portion of the field loss was considered as a supplement to the top soil layer, and the remaining portion was transported to rivers along with water flow and eroded sediments. About 0.59 TBq ^{137}Cs was transported from upland regions to river channels (4), most of which was exported from the catchment in a particulate phase. During the 3.5-y study, the ^{137}Cs reduction rate by wash-off was 1.24 GBq/km^2/y, and the reduction ratio was 1.6% (Table 4). The amount of ^{137}Cs that stored in river sediments was very small, about 4% of the total inflowing ^{137}Cs from upland areas. The natural radioactive decay was about 2.82 TBq (1+3+5). Thus, the ^{137}Cs reduction mainly depended on radioactive decay. If we consider ^{137}Cs reduction by natural radioactive decay, the total loss of ^{137}Cs was 3.39 TBq (1+3+5+6), which indicates that about 90% ^{137}Cs remained in the catchment. Simulated results from Mori et al. (2015) in the Hokkawa Dam watershed also showed most of the ^{137}Cs fallout still remained within the watershed boundary at the end of 2013. This might be a common feature for most watersheds without decontamination works in Fukushima.

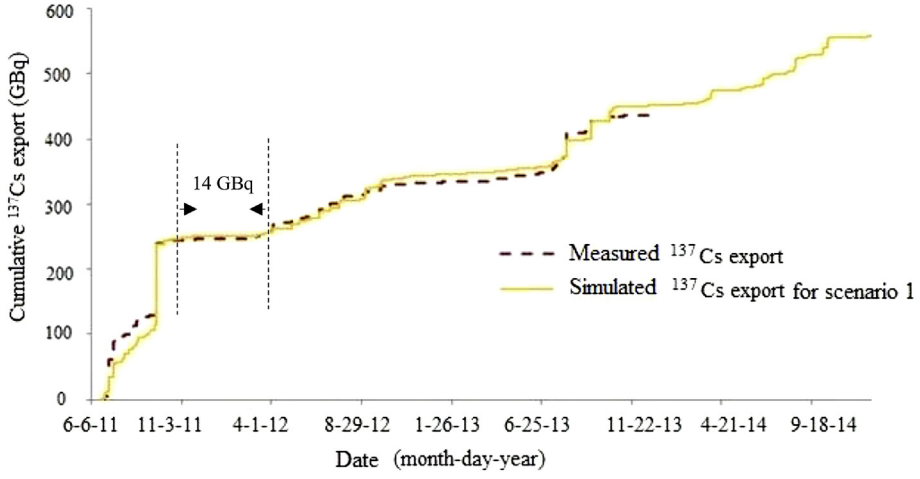

Fig. 8. Cumulative ^{137}Cs transport at the downstream site. (The measured ^{137}Cs export during the period Nov. 2011 ~ Apr. 2012 was about 14 GBq).

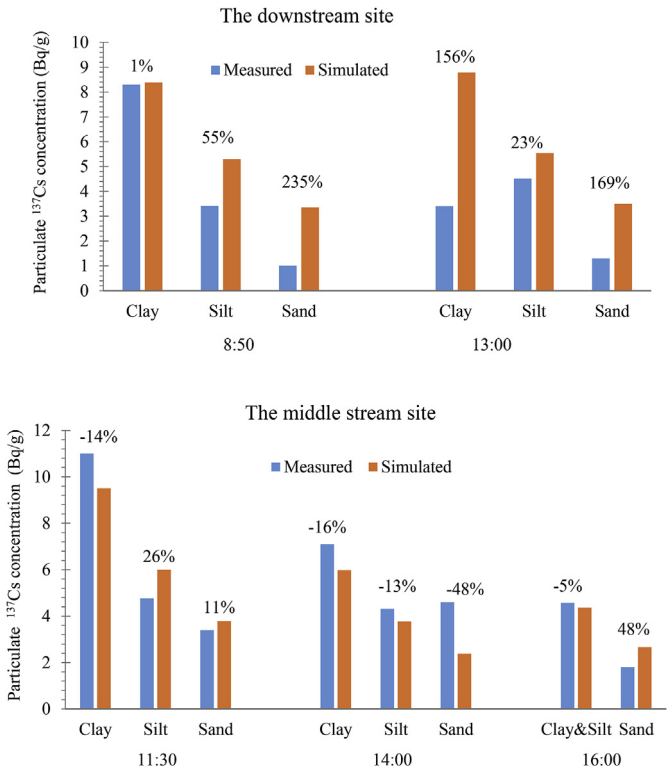

Fig. 9. Comparison of simulated and observed instantaneous ^{137}Cs concentration of suspended sediment (SS) at the downstream site and middle stream site. (Sampling time was 8:50, 13:00, 11:30, 14:00, 16:00 on Oct. 16 2013 respectively. Labeled numbers represent relative percent differences of simulated and measured ^{137}Cs concentration. For the measurement: clay (≤2.7 μm), silt (2.7–63 μm) and sand (63–132 μm). Data in this figure was listed in supplementary table S2.1).

4.4. Spatial patterns of ^{137}Cs transport

Fig. 11 shows the spatial distribution of ^{137}Cs transport in each model grid cell. Areas with the largest net loss of ^{137}Cs are hillsides and areas near river banks (Fig. 3). As a result of sediment deposition, ^{137}Cs accumulated near the source of eroded areas, which may be considered as ^{137}Cs "hotspots" and can be targeted as areas for future decontamination. The spatial identification of ^{137}Cs transport shown in the Fig. 11 should be helpful for developing various decontamination strategies in this catchment.

The catchment was divided into 21 subwatersheds within ArcGIS software to analyze the spatial variation of ^{137}Cs transport. The ^{137}Cs reduction rate and reduction ratio by rainfall–runoff for these subwatersheds were calculated and summarized in Table 4 and appear in Fig. 12 and Fig. 13, respectively. The ^{137}Cs reduction rate demonstrates that the ^{137}Cs inventory in the upper part of the catchment decreased faster than that in the other areas, which corresponds to the initial ^{137}Cs distribution (Fig. 2). In contrast, the ^{137}Cs reduction ratio of the subwatersheds in the middle portion of the catchment was higher.

Spatial variations in ^{137}Cs contamination and soil erosion affect the ^{137}Cs reduction rates and ratios. Particulate ^{137}Cs eroded from soils is the main source of ^{137}Cs in the water flow. Not surprisingly, areas with the most severe soil erosion had the greatest ^{137}Cs reductions (Table 4). Although soil erosion in the upper catchment was of smaller magnitude, ^{137}Cs concentrations of eroding soil particles from those areas were higher. Higher concentration indicates a larger amount of ^{137}Cs per unit of eroded sediment. Consequently, the ^{137}Cs reduction rate in those heavily contaminated subwatersheds was higher. This contrast supplies more information on ^{137}Cs transport behavior beyond the field station observations. Undoubtedly, the ^{137}Cs reduction rate was higher in the upper stream areas. Nevertheless, decontamination works in the critical ^{137}Cs-adsorbed sediment erosion zone including subwatersheds 8, 11, 16 and 20 in the middle portion of the catchment are also urgently needed, particularly for assessment of long-term radiocesium risks.

5. Summary and conclusions

In this study, a watershed-scale ^{137}Cs transport model was developed based on the TREX framework and applied to the

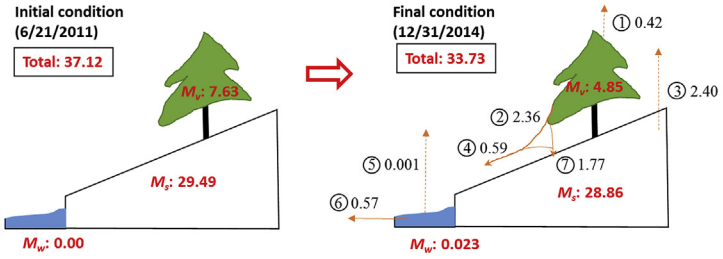

ΔM_v = - ① - ② = - 0.42 – 2.36 = -2.78 (TBq)

ΔM_s = - ③ + ⑦ = - ③ + ② - ④ = - 2.4 + 2.36 – 0.59 = -0.63 (TBq)

ΔM_w = - ⑤ - ⑥ + ④ = - 0.001 - 0.57 + 0.59 = 0.02 (TBq)

ΔM = - ① - ③ - ⑤ - ⑥ = - 0.42 – 2.4 - 0.001 - 0.57 = -3.39 (TBq)

①, ^{137}Cs radioactive decay in the vegetation layer;
②, ^{137}Cs loss from the vegetation layer;
③, ^{137}Cs radioactive decay from ground surface;
④, ^{137}Cs transport from the upland to the river;
⑤, ^{137}Cs radioactive decay in the river;
⑥, ^{137}Cs transport out of the catchment from outlet;
⑦, net incoming of ^{137}Cs in the soil layers because of rainfall-runoff (② - ④);

M_v and ΔM_v, ^{137}Cs amount and ^{137}Cs change in the vegetation layer, respectively;
M_w and ΔM_w, ^{137}Cs amount and ^{137}Cs change in the river, respectively;
M_s and ΔM_s, ^{137}Cs amount and ^{137}Cs change in the soil, respectively;
ΔM, ^{137}Cs change in the catchment;

Fig. 10. Simulated ^{137}Cs distribution in vegetation-soil- river and mass balance of ^{137}Cs transport during the simulation period (units: TBq).

Table 4
Simulated Cesium-137 and suspended sediment (SS) delivery from upland area to the river.

Subwaters-hed No.	Deposited ^{137}Cs (TBq)	^{137}Cs reduction (GBq)	Reduction rate (GBq/km^2/y)	Reduction ratio (%)	SS delivery (t/km^2/year)
1	2.37	40.0	2.06	1.70	123
2	1.95	28.1	1.52	1.45	95
3	5.27	92.3	2.42	1.76	142
4	0.86	11.1	1.01	1.28	206
5	1.15	15.9	1.09	1.38	183
6	5.78	54.9	2.00	0.98	83
7	0.82	9.5	0.96	1.17	64
8	0.89	19.8	1.44	2.18	188
9	1.17	19.2	1.18	1.67	94
10	1.61	29.5	1.24	1.80	116
11	2.47	58.9	1.43	2.38	181
12	2.14	38.4	1.04	1.79	142
13	1.69	24.8	0.81	1.50	179
14	1.84	25.9	1.11	1.38	127
15	0.80	6.7	0.46	0.83	50
16	0.71	20.0	1.49	2.82	337
17	0.65	11.7	0.89	1.83	203
18	1.01	21.5	1.08	2.08	136
19	1.90	14.7	0.34	0.75	222
20	0.79	23.5	1.13	2.91	178
21	1.23	26.7	0.90	2.15	160
Total	37.12	592.9	1.24	1.60	155

Subwatersheds are shown in Fig. 12.

Kuchibuto River catchment. Our simulations indicate that between June, 2011, and December, 2014, the overall ^{137}Cs reduction was 3.39 TBq. Approximately 90% of the initial ^{137}Cs inventory remained in the watershed at the end of 2014. Relative to its initial inventory, ^{137}Cs associated with vegetation was subject to the largest reduction, with approximately 30% of the radiocesium initially present being redistributed elsewhere and a small portion lost by radioactive decay. Approximately 75% of the radiocesium washed off vegetation was incorporated into surface soils, where it is largely available for transport with soil particles as they erode, particularly silts. An estimated 4.85 TBq of ^{137}Cs remained in vegetation at the end of 2014 and washoff will continue to contribute to radiocesium export for several decades. Over the 3.5-year period, 0.57 TBq of ^{137}Cs was exported from the catchment, primarily by wash-off and soil erosion with a clay, silt, and sand ratio of 17:70:13, respectively. The average ^{137}Cs reduction rate by rainfall–runoff wash-off was 1.24 GBq/km^2/y, corresponding to 1.6% of the initial radiocesium inventory of the watershed. Cycles of erosion and redeposition driven by large rainfall events are expected to continue to transport radiocesium from upland areas to more populated areas downstream. These simulations indicate areas within the watershed where radiocesium accumulates, providing a tool that could be used to evaluate risk management alternatives such as targeted decontamination.

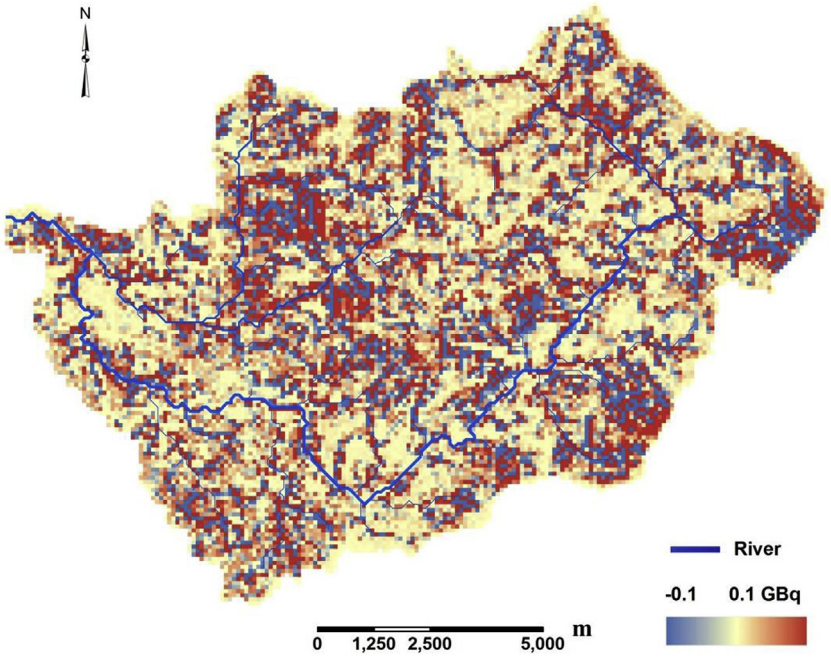

Fig. 11. Simulated spatial distribution of ^{137}Cs dynamics on the upland regions in the case of scenario 1. Negative values indicate decreases in ^{137}Cs.

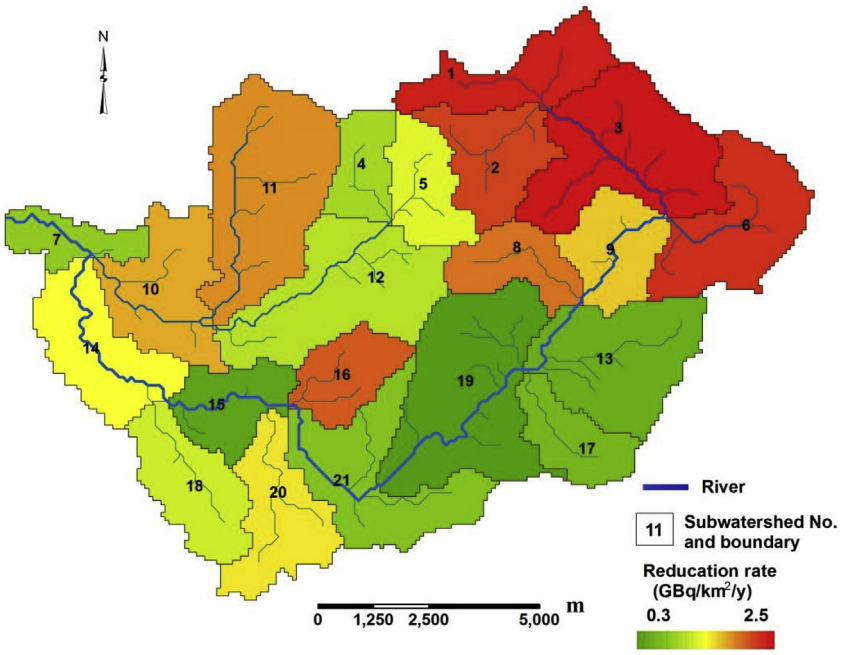

Fig. 12. Simulated spatial distribution of ^{137}Cs reduction rate by wash-off in the case of scenario 1: June 2011–December 2014.

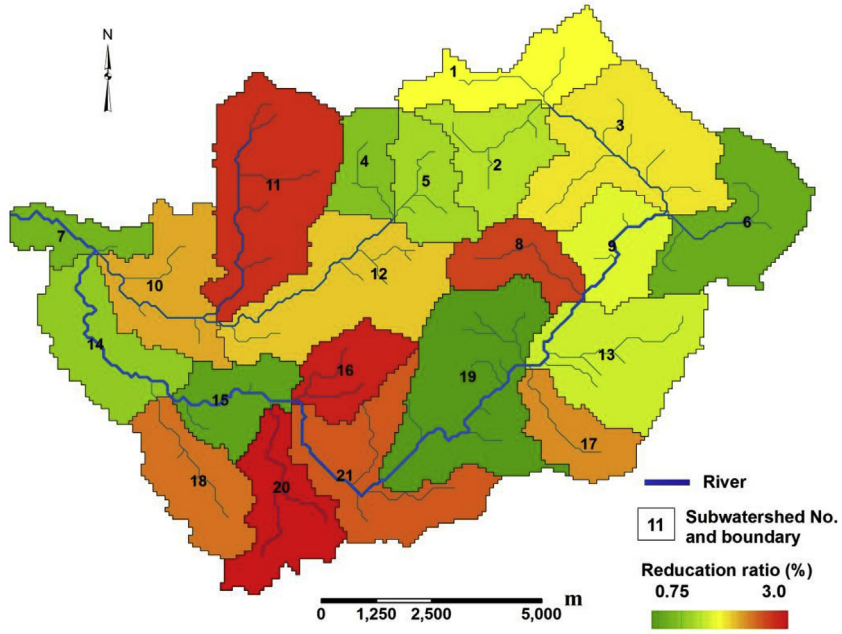

Fig. 13. Simulated spatial distribution of ^{137}Cs reduction ratio by wash-off in the case of scenario 1: June 2011–December 2014.

Acknowledgments

This work was financially supported by the Ministry of Education, Culture, Sports, Science and Technology (MEXT) as a Grant-in Aid for Scientific Research (No. 25110503) and the Japan Atomic Energy Agency (JAEA) as a part of the MEXT-funded project entitled "the establishment of grasp method of long-term effects caused by radioactive materials from the Fukushima Dai-ichi Nuclear Power Plant accident". The authors thank Prof. Yuichi Onda (the University of Tsukuba) for providing some flow rate and sediment concentration data, and Mr. Teppei Omata, Ms. Megumi Araya, Mr. Keiichi Takahashi for helping to do sample collections and measurements. We are grateful to the editor and two anonymous reviewers for constructive reviews.

Appendix A. Supplementary data

Supplementary data related to this article can be found at http://dx.doi.org/10.1016/j.jenvrad.2017.01.017.

References

Ayabe, Y., Kanasashi, T., Hijii, N., Takenaka, C., 2014. Radiocesium contamination of the web spider Nephila clavata (Nephilidae: Arachnida) 1.5 years after the

Fukushima Dai-ichi nuclear power plant accident. J. Environ. Radioact. 127, 105–110.
Chadwick, R.C., Chamberlain, A.C., 1970. Field loss of radionuclides from grass. Atmos. Environ. 4, 51–56.
England, J., Velleux, M.L., Julien, P.Y., 2007. Two-dimensional simulations of extreme floods on a large watershed. J. Hydrol. 347, 229–241.
Ertel, J., Voigt, G., Paretzke, H.G., 1989. Weathering of $^{134/137}$Cs following leaf contamination of grass cultures in an outdoor experiment. Radiat. Environ. Biophys. 28, 319–326.
FAJ (Forestry Agency of Japan), 2012. Preliminary Results of Surveys of Distributions of Radioactive Elements in Forest Ecosystems. http://www.rinya.maff.go.jp/j/press/hozen/111227_2.html.
Fan, Q.H., Tanaka, M., Tanaka, K., Sakaguchi, A., Kondo, H., Takahashi, Y., 2014. Factors controlling radiocesium distribution in river sediments: field and laboratory studies after the Fukushima Dai-Ichi nuclear power plants accident. Appl. Geochem. 48, 93–103.
Fraley Jr., G., Chavez, L., Markham, O.D., 1993. Seasonal variations in deposition and retention of cerium-141 and cesium-134 in cool desert vegetation. J. Environ. Radioact. 21 (3), 203–212.
Garcia-Sanchez, L., 2008. Watershed wash-off of atmospherically deposited radionuclides: review of the flux. J. Environ. Radioact. 99 (4), 563–573.
Harada, K., Fujii, Y., Adachi, A., Tsukidate, A., Asai, F., Koizumi, A., 2013. Dietary intake of radioactive cesium in adult residents in Fukushima prefecture and neighboring regions after the Fukushima nuclear power plant accident: 24 hr -food duplicate survey in december 2011. Environ. Sci. Technol. 47 (6), 2520–2526.
He, Q., Walling, D.E., 1996. Interpreting particle size effects in the adsorption of ^{137}Cs and unsupported ^{210}Pb by mineral soils and sediments. J. Environ. Radioact. 30, 117–137.
IAEA, 15 September 2011. Additional report of Japanese Government to IAEA—accident at TEPCO's Fukushima nuclear power stations transmitted by nuclear emergency response headquarters, Government of Japan. International Atomic Energy Agency (IAEA). Accessed online (July 1, 2012): http://www.iaea.org/newscenter/focus/fukushima/japan-report2/.
IAEA, 2007. Report on the IAEA-CU-2006-03 World-wide Proficiency Test on the Determination of Gamma Emitting Radionuclides. May 2007 (IAEA/AL/171). International Atomic Energy Agency (IAEA), Vienna.
JAEA (Japan Atomic Energy Agency), 2014. Annual Report on "research on Distribution of the Radioactive Materials from the Fukushima Dai-ichi Nuclear Power Plant Accident" (Chapter 2.6). http://133.188.30.97/initiatives/cat03/entry06.html.
Ji, U., Velleux, M., Julien, P., Hwang, M., 2014. Risk assessment of watershed erosion at Naesung Stream, South Korea. J. Environ. Man. 136 (1), 16–26.
Julien, P.Y., Saghafian, B., Ogden, F.L., 1995. Raster-based hydrologic modeling of spatially-varied surface runoff. Water Resour. Bull. 31, 523–536.
Julien, P.Y., Rojas, R., 2002. Upland erosion modeling with CASC2DSED. Int. J. Sed. Res. 17 (4), 265–274.
Julien, P.Y., Saghafian, B., 1991. CASC2D User's Manual – a Two Dimensional Watershed Rainfall-runoff Model. Civil Eng. Report CER90-91PYJ-BS-12. Colorado State University, Fort Collins, CO.
Kanasashi, T., Sugiura, Y., Takenaka, C., Hijii, N., Umemura, M., 2015. Radiocesium distribution in sugi (Cryptomeria japonica) in Eastern Japan: translocation from needles to pollen. J. Environ. Radioact. 139, 398–406.
Kato, H., Onda, Y., Gomi, T., 2012. Interception of the Fukushima reactor accident derived ^{137}Cs, ^{134}Cs and ^{131}I by coniferous forest canopies. Geophys. Res. Lett. 39, L20403. http://dx.doi.org/10.1029/2012GL052928.
Kinouchi, T., and Musiake, K., Simulating hydrological impact of environmental change in the Abukuma Watershed, Japan. 4th APHW Conference. 2008.
Kinouchi, T., Yoshimura, K., Omata, T., 2015. Modeling radiocesium transport from a river catchment based on a physically-based distributed hydrological and sediment erosion model. J. Environ. Radioact. 139, 407–415.
Kivva, S.L., Zheleznyak, M.I., 2000. Hydrological and physico-chemical processes determining radionuclide redistribution. In: van der Perck, M., Svetlitchnyi, A.A., den Basten, J., Wielinga, A. (Eds.), ARTACUS, Spatial Redistribution of Radionuclides within Catchments. Final Report EC Contract No. IC15CT980215. Utrecht University, The Netherlands, pp. 13–16.
Kitamura, A., Yamaguchi, M., Kurikami, H., Yui, M., Onishi, Y., 2014. Predicting sediment and cesium-137 discharge from catchments in eastern Fukushima. Anthropocene 5, 22–31.
Kobayashi, S., Shinomiya, T., Kitamura, H., Ishikawa, T., Imaseki, H., Oikawa, M., Kodaira, S., Miyaushiro, N., Takashima, Y., Uchihori, Y., 2015. Radioactive contamination mapping of northeastern and eastern Japan by a car-borne survey system, Radi-Probe. J. Environ. Radioact. 139, 281–293.
Loffredo, N., Onda, Y., Kawamori, A., Kato, H., 2014. Modeling of leachable ^{137}Cs in throughfall and stemflow for japanese forest canopies after Fukushima dai-ichi nuclear power plant accident. Sci. Total Environ. 493, 701–707.
Loffredo, N., Onda, Y., Hurtevent, P., Coppin, F., 2015. Equation to predict the ^{137}Cs leaching dynamic from evergreen canopies after a radio-cesium deposit. J. Environ. Radioact. 147, 100–107. http://dx.doi.org/10.1016/j.jenvrad.2015.05.018.
Masson, O., Baeza, A., Bieringer, et al., 2011. Tracking of airborne radionuclides from the damaged Fukushima Dai-Ichi nuclear reactors by European Networks. Environ. Sci. Technol. 45, 7670–7677. http://dx.doi.org/10.1021/es2017158.
Madoz-Escande, C., Garcia-Sanchez, L., Bonhomme, T., Morello, M., 2005. Influence of rainfall characteristics on elimination of aerosols of cesium, strontium, barium and tellurium deposited on grassland. J. Environ. Radioact. 84, 1–20.
Matsunaka, T., Sasa, K., Sueki, K., Takahashi, T., Satou, Y., Matsumura, M., Kinoshita, N., Kitagawa, J., Matsuzaki, H., 2016. Pre- and post-accident ^{129}I and ^{137}Cs levels, and ^{129}I/^{137}Cs ratios in soil near the Fukushima Dai-ichi Nuclear Power Plant, Japan. J. Environ. Radioact. 151, 209–217.
MEXT, 2013. Extension Site of Distribution Map of Radiation Dose, Etc. http://ramap.jmc.or.jp/map/eng/.
Milbourn, G.M., Taylor, R., 1965. The contamination of grassland with radioactive strontium I. Initial retention and loss. Radiat. Bot. 5, 337–347.
Monte, L., 2001. A generic model for assessing the effects of countermeasures to reduce the radionuclide contamination levels in abiotic components of fresh water systems and complex catchments. Environ. Model. Softw. 16, 669–690.
Mori, K., Tada, K., Tawara, Y., Ohno, K., Asami, M., Kosaka, K., Tosaka, H., 2015. Integrated watershed modeling for simulation of spatiotemporal redistribution of post-fallout radionuclides: application in radiocesium fate and transport processes derived from the Fukushima accidents. Environ. Modell. Softw. 72, 126–146. http://dx.doi.org/10.1016/j.envsoft.2015.06.012.
Moriasi, D.N., Arnold, J.G., Van Liew, M.W., Bingner, R.L., Harmel, R.D., Veith, T.L., 2007. Model evaluation guidelines for systematic quantification of accuracy in watershed simulations. Trans. ASABE 50 (3), 885–900.
Nagao, S., Kanamori, M., Ochiai, S., Tomihara, S., Fukushi, K., Yamamoto, M., 2013. Export of ^{134}Cs and ^{137}Cs in the Fukushima river systems at heavy rains by typhoon Roke in september 2011. Biogeosci. Discuss. 10, 2767–2790.
Phillips, J.M., Russell, M.A., Walling, D.E., 2000. Time-integrating sampling of fluvial suspended sediment: a simple methodology for small catchments. Hydrol. Process 14, 2589–2602.
Rojas, R., Velleux, M., Julien, P., Johnson, B., 2008. Grid scale effects on watershed soil erosion models. J. Hydrol. Eng. 13 (9), 793–802.
Saito, K., Tanihata, I., Fujiwara, M., Saito, T., Shimoura, S., Otsuka, T., Onda, Y., Hoshi, M., Ikeuchi, Y., Takahashi, F., Kinouchi, N., Saegusa, J., Seki, A., Takemiya, H., Shibata, T., 2015. Detailed deposition density maps constructed by large-scale soil sampling for gamma-ray emitting radioactive nuclides from the Fukushima Dai-ichi Nuclear Power Plant accident. J. Environ. Radioact. 139, 308–319.
Sakaguchi, A., Tanaka, K., Iwatani, H., Chiga, H., Fan, Q., Onda, Y., Takahashi, Y., 2014. Size distribution studies of ^{137}Cs in river water in the Abukuma riverine system following the Fukushima Dai-ichi Nuclear Power Plant accident. J. Environ. Radioact. 139, 379–389.
Sasaki, Y., Funaki, H., Iri, S., Dohi, T., Hagiwara, H., 2016. Fate of radiocesium in freshwater aquatic plants and algae in the vicinity of the Fukushima Dai-ichi nuclear power plant. Limnology. http://dx.doi.org/10.1007/s10201-015-0471-6. Published online: January 20.
Sanada, Y., Torii, T., 2015. Aerial radiation monitoring around the Fukushima Dai-ichi nuclear power plant using an unmanned helicopter. J. Environ. Radioact. 139, 294–299.
Sato, I., Okada, K., Sasaki, J., Chida, H., Satoh, H., Miura, K., Kikuchi, K., Otani, K., Sato, S., 2014. Distribution of radioactive cesium and stable cesium in cattle kept on a highly contaminated area of Fukushima nuclear accident. Animal Sci. J. http://dx.doi.org/10.1111/asj.12345.
Shaw, G., 2007. Radionuclides in forest ecosystems. In: George, S. (Ed.), Radioact. Environ. [Internet]. Elsevier, pp. 127–155.
Sheppard, S., Long, J., Sanipelli, B., Sohlenius, G., 2009. Solid/liquid Partition Coefficients (Kd) for Selected Soils and Sediments at Forsmark and Laxemar-simpevarp. Svensk Kärnbränslehantering AB (Swedish Nuclear Fuel and Waste Management Co), Stockholm. SKB Report-09–27. 72 pp.
Stohl, A., Seibert, P., Wotawa, G., Arnold, D., Burkhart, J., Eckhardt, S., Tapia, C., Vargas, A., Yasunari, T., 2012. Xenon-133 and caesium-137 releases into the atmosphere from the Fukushima Dai-ichi nuclear power plant: determination of the source term, atmospheric dispersion, and deposition. Atmos. Chem. Phys. 12, 2313–2343.
Taira, Y., Hayashida, N., Yamaguchi, H., Yamashita, S., Endo, Y., Takamura, N., 2012. Evaluation of environmental contamination and estimated radiation doses for the return to residents' homes in Kawauchi village, Fukushima prefecture. PLoS One 7 (9), e45816. http://dx.doi.org/10.1371/journal.pone.0045816.
Takahashi, J., Tamura, K., Suda, T., Matsumura, R., Onda, Y., 2015. Vertical distribution and temporal changes of ^{137}Cs in soil profiles under various land uses after Fukushima Dai-ichi Nuclear Power Plant Accident. J. Environ. Radioact. 139, 351–361.
Tanaka, K., Iwatani, H., Sakaguchi, A., Takahashi, Y., Onda, Y., 2014. Relationship between particle size and radiocesium in river suspended sediment related to the Fukushima Dai-ichi Nuclear Power Plant accident. J. Radioanal. Nucl. Chem. 301 (2), 607–613.
Tanaka, T., Tachikawa, Y., Shiiba, M., Yorozu, K., Kim, S., 2013. Numerical modeling and estimation of radioactive cesium movement at the Kuchibuto river basin, Fukushima. Journal of Japan Society of Civil Engineers. Ser. B1 Hydraul. Eng. 69, 1_487–1_492.
Ueda, S., Hasegawa, H., Kakiuchi, H., Akata, N., Ohtsuka, Y., Hisamatsu, S., 2013. Fluvial discharges of radiocaesium from watersheds contaminated by the Fukushima dai-ichi nuclear power plant accident. Jpn. J. Environ. Radioact. 118, 96–104.
van der Perk, M., Slávik, O., 2003. Simulation of event-based and long-term spatial redistribution of Chernobyl-derived radiocaesium within catchments using geographical information system embedded models. Hydrol. Process. 17, 943–957.
Velleux, M., Julien, P.Y., Rojas-Sanchez, R., Clements, W.H., England, J.F., 2006.

Simulation of metals transport and toxicity at a mine impacted watershed: California Gulch, Colorado. Environ. Sci. Technol. 40 (22), 6996–7004.
Velleux, M., England, J., Julien, P., 2008. TREX: spatially distributed model to assess watershed contaminant transport and fate. Sci. Total Environ. 404 (1), 113–128.
Velleux, M., Redman, A., Paquin, P., Santore, R., England, J., Julien, P., 2012. Exposure assessment framework for antimicrobial copper use in urbanized areas. Environ. Sci. Technol. 46 (12), 6723–6732.
Wei, L., Kinouchi, T., 2014. Improvement of CASC2D model for rainfall-runoff simulation in a forested catchment. J. Jpn. Soc. Civ. Eng. Ser. B1 Hydraulic Eng. 70 (4), 157–162.
Wei L., Kinouchi T., Velleux M., Omata T., Takahashi K. and Araya M., Soil erosion and transport simulation and critical erosion area identification in a headwater catchment contaminated by the Fukushima nuclear accident, (submitted).
Woolhiser, D.A., Smith, R.E., Goodrich, D.C., 1990. KINEROS, A Kinematic Runoff and Erosion Model: Documentation and User Manual. U S. Department of Agriculture, Agriculture Research Service, ARS-77, 130 p.
Yamaguchi, M., Kitamura, A., Oda, Y., Onishi, Y., 2014. Predicting the long-term ^{137}Cs distribution in Fukushima after the Fukushima Dai-ichi nuclear power plant accident: a parameter sensitivity analysis. J. Environ. Radioact. 135, 135–146.
Yamaguchi, M., Maekawa, K., Takeuchi, S., Kitamura, A., Onishi, Y., 2013. Development of a model to predict a radionuclide distribution based on soil migration after Fukushima Dai-ichi Nuclear Power Plant accident. J. Nucl. Fuel. Cycle Environ. 20, 53–69.
Yamashiki, Y., Onda, Y., Smith, H.G., Blake, W.H., Wakahara, T., Igarashi, Y., Matsuura, Y., Yoshimura, K., 2014. Initial flux of sediment-associated radiocesium to the ocean from the largest river impacted by Fukushima Dai-ichi Nuclear Power Plant. Sci. Rep. 4, 3714. http://dx.doi.org/10.1038/srep03714.